Point-bar brink and channel thalweg trajectories depicting interaction between vertical and lateral shifts of microtidal channels in the Venice Lagoon (Italy)

MARTA COSMA[a], MASSIMILIANO GHINASSI[a], ANDREA D'ALPAOS[a], MARCELLA RONER[a], ALVISE FINOTELLO[a], LAURA TOMMASINI[a], ROBERTO GATTO[a]

[a] Department of Geosciences, University of Padova, Via Gradenigo 6, 35131 Padova, Italy

CORRESPONDING AUTHOR: Marta Cosma marta.cosma@phd.unipd.it

ABSTRACT

Tidal point bars are generally described as laterally accreting bodies, generated by lateral shift of meander bends, in which the point-bar brink (i.e. the break between bar top and bar slope) and the channel thalweg (i.e. the deepest part of the channel) shift horizontally toward the outer bank. The present study applies the concept of trajectory analysis at the point bar scale, focusing on the trajectories of point-bar brink and channel thalweg, in order to understand how vertical aggradation can interact with lateral migration to shape geometries of tidal point bars developed in a microtidal and highly aggrading salt marsh setting. We selected eight study-case meander bends, located in the Venice Lagoon and characterized by different point-bar morphologies, whose widths and depths range from 2 to 11 m and from 0.5 to 1.6 m, respectively. All the point bars were investigated through a high resolution facies-analysis carried out on closely-spaced sediment cores, collected along the bar axis. Location of bar brink and channel thalweg at different times defined specific trajectories, which were classified either as ascending or descending, and linear or non-linear. All brink trajectories are ascending, and show evidence of lateral shift of the bar brink under aggradational conditions of surrounding marshes. Development of non-linear brink trajectories is linked with changes in the ratio between vertical and lateral shift rates of the brink, which is in turn dictated by changes in local base level due to substrate compaction. Conversely, the thalweg trajectories can be either ascending or descending, reflecting an interaction between rates of lateral shift and aggradation/degradation of the channel floor. The brink and thalweg can either shift consistently (e.g., both trajectories are ascending) or incongruously (e.g., ascending brink vs. descending thalweg trajectory), reflecting different attitudes of the channel to maintain or increase its cross-sectional area.

Keywords: tidal point bar, aggradation, channel thalweg, lateral migration

1. INTRODUCTION

Trajectory analysis focuses on the migration pattern of easily recognizable geomorphological features (e.g., breaks-in-slope) and associated sedimentary environments through time (cf. Helland-Hansen and Hampson, 2009). This approach is suitable to be applied to a large variety of scales, which can range from bedforms (cf. “climb angle” by Larue and Martinez, 1989) to continental margins (Henriksen et al., 2011). In addition, trajectory analysis has been widely employed at the shoreline or shelf-edge scale, shedding light on the distribution of different depositional systems through time in response to combined variations in rates of relative sea level changes and sediment supply (Henriksen et al., 2009, and reference therein). On the contrary, less attention has been paid at the scale of depositional elements, like deltas (Gobo et al., 2015) or fluvial bars (Ghinassi et al., 2014).

Point bars generated by fluvial and tidal meandering channels are mostly described as laterally accreting bodies (Bridges and Leeder, 1976; Colombera et al., 2017; D’Alpaos et al., 2017; Durkin et al., 2015; Fisk, 1944; Jackson, 1976; McGowen and Garner, 1970; Miall, 1985; Smith, 1987) with a tabular geometry. This geometry is generated by lateral shift of the inner channel bank, which implies a synchronous horizontal shift (Fig. 1A) of both the bar brink (i.e. the morphological break between bar top and bar slope) and the channel thalweg (i.e. the deepest part of the channel), which, in a cross section parallel to the bend axis, defines two parallel and horizontal trajectories (Fig 1A). Although the common occurrence of tabular point-bar bodies in the stratigraphic record (Pranter et al., 2007; Puigdefabregas, 1973; Puigdefabregas and Van Vliet, 1977) supports this model, documentations of stable to slow-migrating channels in high-aggradational settings (Candel et al., 2017; Ielpi et al., 2015; Makaske, 2001; Nanson and Croke, 1992) suggest that a high ratio between vertical and lateral accretion rate is likely to promote a mixed, latero-vertical shift of meandering channel systems.

Fluvial meanders migrate laterally with a mean rate of meters per year (Bridge et al., 1995; Hudson and Kesel, 2000; Lagasse et al., 2004), although this rate can vary from being undetectable over decades (Beeson and Doyle, 1995; Candel et al., 2017; Hudson and Kesel, 2000) to reach values as high as tens of meters during a single flood event (Ghinassi et al., 2018b; Moody and Meade, 2014). The interaction between rate of vertical and lateral shift of fluvial meanders has been rarely documented in the stratigraphic record (Ghinassi et al., 2014; Ielpi et al., 2015; Rajchl and Uličný, 2005), and numerical models (van de Lageweg et al., 2016; Willis and Tang, 2010) show that only high overbank aggradation rates (i.e. cm/yr to dm/yr) might possibly affect geometries of point bar bodies. Fluvial meanders developed by high sinuosity, low-energy streams in peatlands of the Netherlands (Candel et al., 2017) represent an end-member of interaction between rate of vertical and lateral shift of meandering channels. In this setting, geometries of bar bodies are prominently shaped by vertical accretion through processes of oblique aggradation (cf. Candel et al., 2017), which cause the bar brink and channel thalweg to shift synchronously following steep to vertical trajectories. Rajchl and Uličný (2005) analyzed the influence of substrate compaction on geometries of point bar bodies recorded in the Neogene Hrabák fluvial system in the Most Basin (Czech Republic).

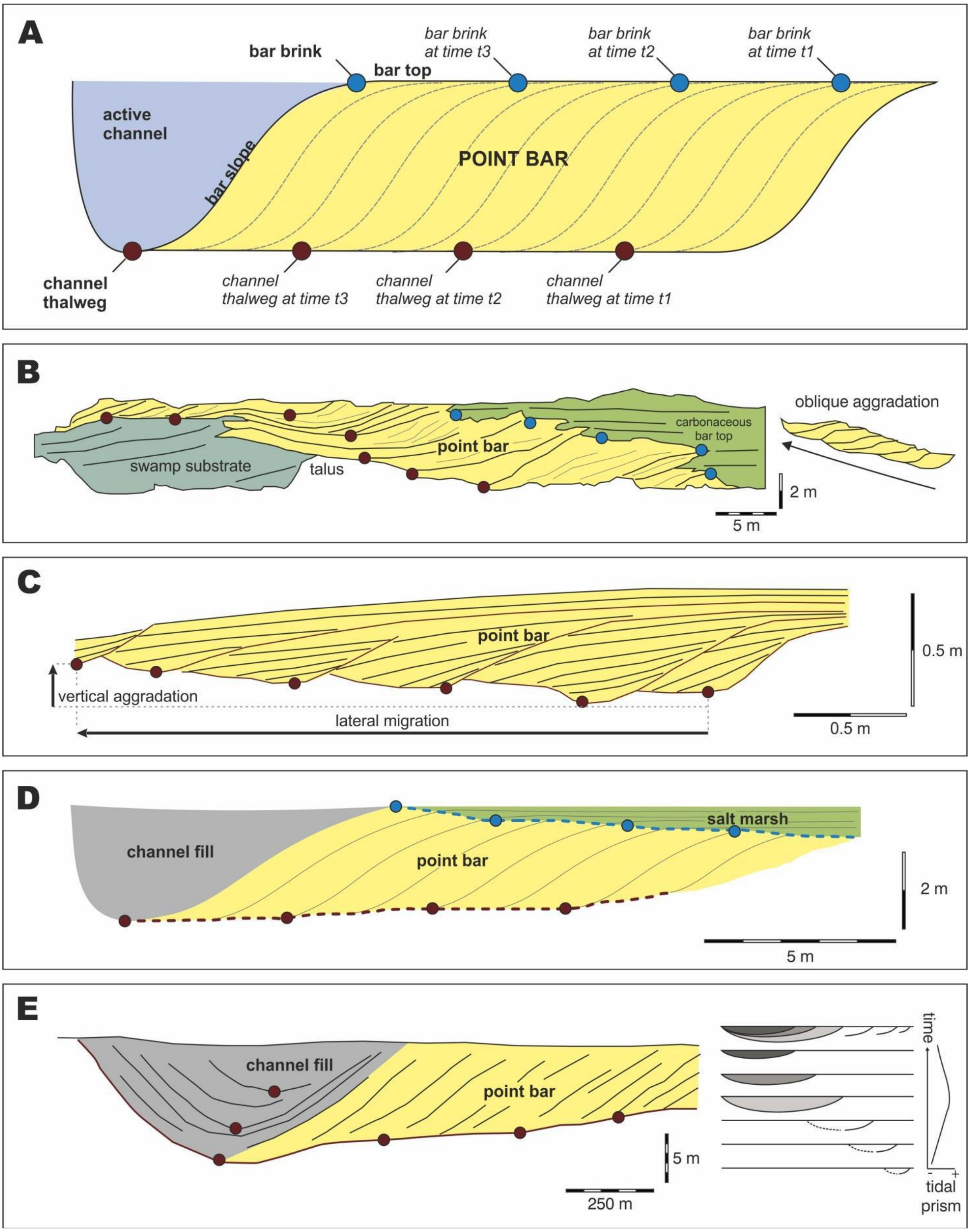

Figure 1 Models for point bar geometries. (A) Idealized model showing stratal geometries generated by lateral shift of the point bar brink and channel thalweg. (B) Lateral and vertical shift of a fluvial point bar of the Neogene Hrabák system, Czech Republic (modified after Rajchl and Uličný, 2005). (C) Channel thalweg migration under aggradational conditions in a modern tidal meander bend of the Drum Bay, Scotland

(modified after De Mowbray, 1983). (D) Brink and thalweg trajectories of a modern tidal point bar in the Venice Lagoon (modified from Brivio et al., (2016). (E) Channel thalweg trajectory under the effect of a changing tidal prism in a Mid-Holocene channel, Netherlands (modified from Rieu et al., (2005)

They showed that syndepositional compaction of peat deposits, due to sediment loading of the overlying growing point bars, leads to a local increase in subsidence, which causes development of steep brink and channel thalweg trajectories (Fig 1B).

Similarly to their fluvial counterparts, tidal point bars were commonly described (Barwis, 1978; Bridges and Leeder, 1976) as tabular sedimentary bodies generated by horizontal and synchronous shift of bar brink and channel thalweg. Nevertheless, as demonstrated for fluvial systems, lateral migration of tidal meanders can follow different styles, and the trajectories defined by both point bar brink and channel thalweg are not necessarily horizontal nor parallel. As a matter of example, De Mowbray (1983) showed that the channel thalweg of a tidal meander bend in the Drum Bay (Scotland) did not merely shifted horizontally, but migrated under gradual aggradation (Fig 1C) in order to keep pace with the build-up of the adjacent tidal flats. A similar behavior was also documented by Brivio et al. (2016) for the brink of a modern tidal point bar in the Venice Lagoon (Italy), where a combination between channel lateral shift and aggradation of the surrounding saltmarshes caused the bar brink to rise during the channel lateral shift (Fig 1D). Finally, using high-resolutions seismic data from western Netherlands, Rieu et al. (2005) described a lateral shift of a mid-Holocene tidal channel under the effect of varying tidal prism. In this case, the shift of the channel thalweg defined a descending and ascending trajectory during phases of increase and decrease in the tidal prism, respectively (Fig 1E).

It emerges that, during lateral migration of tidal channels, the shift of the bar brink and the channel thalweg may not be horizontal and in phase, being their behaviour dictated by the interaction between different factors, which include rate of channel lateral shift (e.g. D’Alpaos et al., 2017; Fagherazzi et al., 2004; Finotello et al., 2018), rate of vertical aggradation of adjacent unchanneled areas (e.g. D’Alpaos et al., 2007), local variations of relative sea level and the related increase/decrease in tidal prism (e.g. D’Alpaos et al., 2010). The combinations between different types of bar brink and channel thalweg trajectories, along with the related changes of point bar thickness and geometry, can provide relevant insight on the identification of the depositional boundary conditions under which bend migration occurred. Therefore, describing different bar brink and thalweg trajectories, as well as of their possible combinations, is a critical step towards an improved understanding of the morphodynamic evolution of tidal meanders and related sedimentary products. These issues are mostly relevant in tidal landscapes, where highly aggradational (i.e. cm/yr) marshes host a complex network of slowly-migrating (i.e. cm to dm/yr) meandering channels (Allen, 2000; Fagherazzi et al., 2004; Gabet, 1998; Garofalo, 1980; Hughes, 2012; Marani et al., 2002), whose sedimentary and architectural features are still relatively unexplored (Boaga et al., 2018; D’Alpaos et al., 2017; Ghinassi et al., 2018a). The present work focuses on meander bends of the Venice Lagoon providing the first description of different styles of bar brink and channel thalweg trajectories in order to improve our understanding of tidal point-bar evolution and architecture. Specifically, this study aims at i) illustrating geometries of tidal point bars along 2D axial cross sections; and ii) defining the behavior of the bar brink and channel thalweg where point bar bodies accrete under aggradational conditions.

2. THE VENICE LAGOON AND THE STUDY SITES

The Venice Lagoon is located along the Northeastern coast of Italy, it has a total surface of about 550 km^2 and represents the largest brackish water body of the Mediterranean Basin (Fig 2A). The Lagoon is characterized by an elongated shape trending NE-SW and by a mean water depth of tidal flat and subtidal platform of about 1.5 m. It is connected to the Adriatic Sea through three inlets: Lido, Malamocco, and Chioggia (Fig 2A). The tidal regime is semidiurnal with an average range of about 1.0 m. The maximum water excursion at the inlets is ±0.75 m around Mean Sea Level (MSL) (D'Alpaos et al., 2013) which can be increased by meteorological forcing (Carniello et al., 2016).

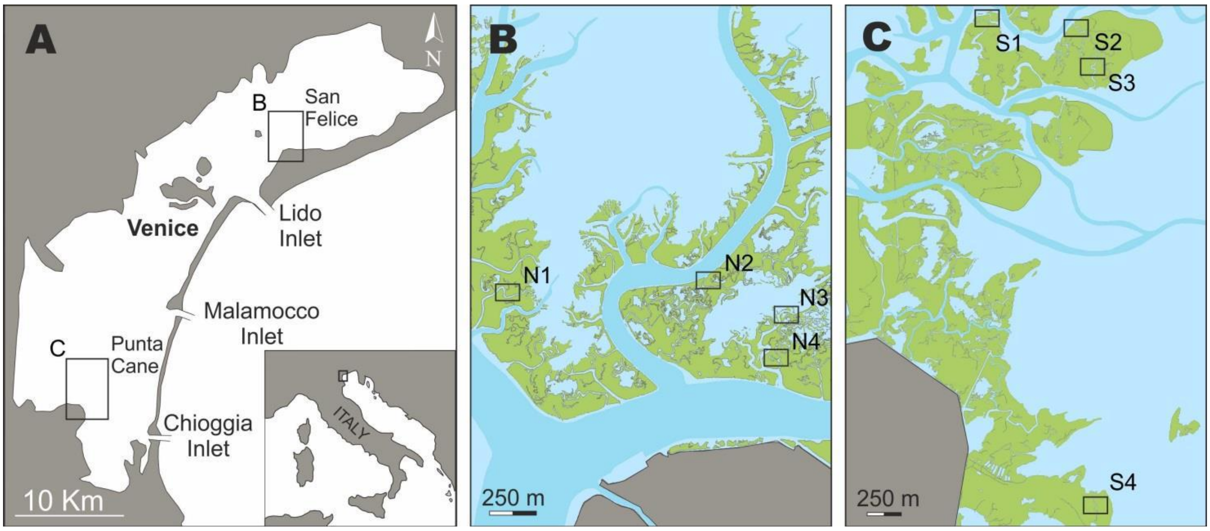

Figure 2 Study sites. (A) Location of the Venice Lagoon along the Northeastern coast of Italy. (B and C) Location of the study sites in the Northern (N1, N2, N3, and N4) and Southern (S1, S2, S3, and S4) Venice Lagoon, respectively.

The Venice Lagoon is part of a wider foreland basin located between the Apennine and the South Alpine chains (Massari et al., 2009). The Quaternary infill of the basin, in the Venice area, consists of a shallowing upward trend from deep marine hemipelagic mud and turbiditic succession to deltaic and shoreface deposits

(Massari et al., 2004), which is followed by a cyclic alternation of continental to shallow marine facies deposited under glacio-eustatic control in the uppermost succession (Kent et al., 2002). The last recorded cycle consists of the alluvial sediments of the Brenta River Megafan, developed in the area during the Last Glacial Maximum (Fontana et al., 2014), and of the lagoonal deposits related to the Holocene transgression, which prompted paralic deposition and the development of the Venice Lagoon (Amorosi et al., 2008; Zecchin et al., 2014, 2008). During the last five centuries, human interventions have strongly altered the natural evolution of the Lagoon, preventing its siltation (D'Alpaos, 2010; Gatto and Carbognin, 1981), and causing a human-induced transgressive phase (Zecchin et al., 2014, 2009, 2008), which is associated with a significant reduction in salt marsh surface (D'Alpaos, 2010; Day et al., 1998; Marani et al., 2007; Roner et al., 2016).

Nowadays, the great majority of salt marshes are found in the Southwestern and Northwestern areas of the Lagoon. Salt marshes located in the Northern Venice Lagoon have been characterized by accretion rates ranging between 0.1 and 0.5 cm/yr during the last century, with the highest values observed after the 1960s (Bellucci et al., 2007). Conversely, the accretion rates of salt marshes located in the Southern Venice Lagoon ranged between 0.1 and 1.2 cm/yr since the 14th century, when palustrine sedimentation ceased and salt marshes colonization began (Roner et al., 2017).

The present study focuses on eight different meander bends, four of which (N1 –N4, Fig 2B) cut through the San Felice salt marshes in the Northern Lagoon, whereas the others are located in the Southwestern marshes of Punta Cane (S1 – S4, Fig 2C).

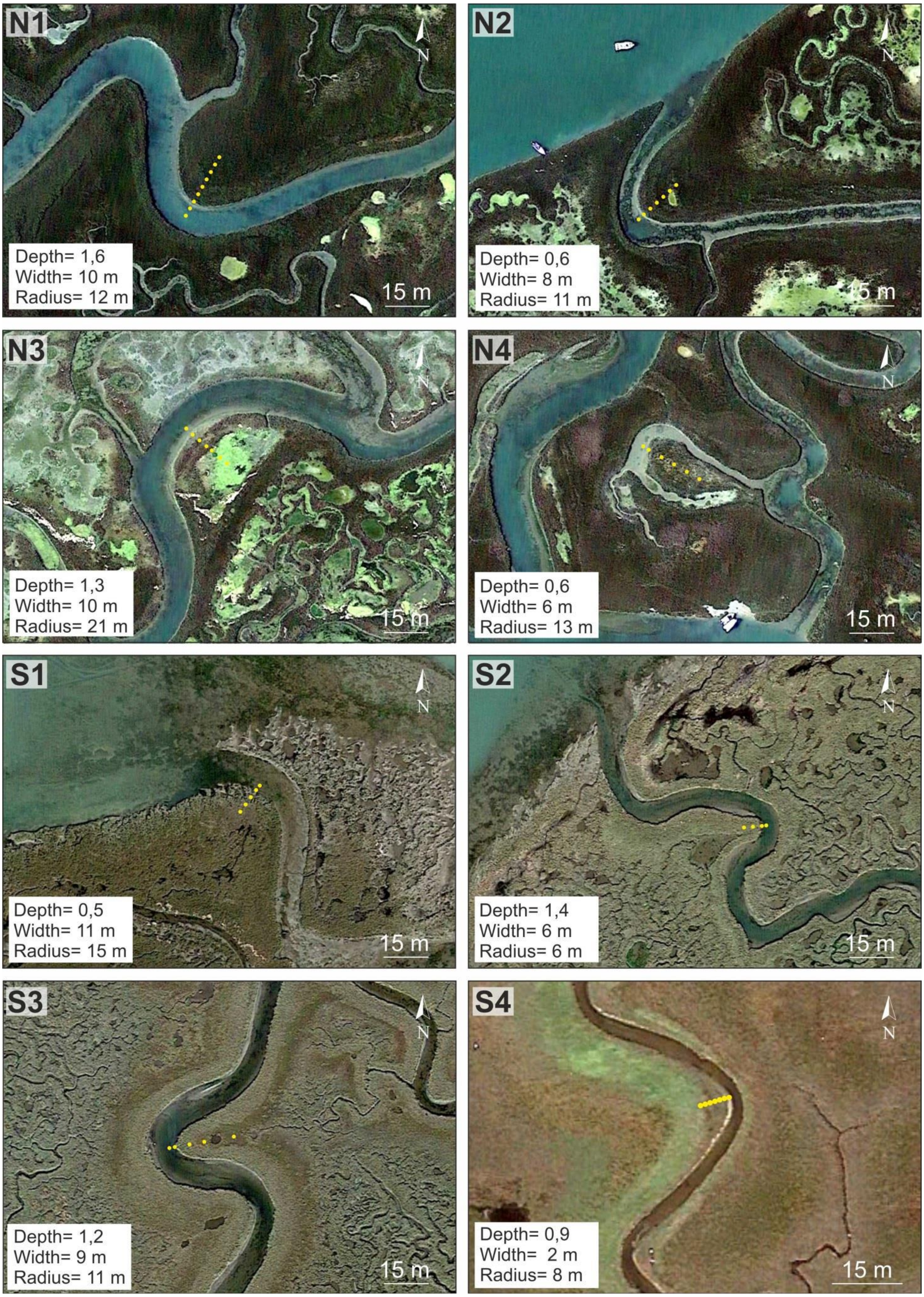
N1
Depth= 1,6
Width= 10 m
Radius= 12 m
15 m
N2
Depth= 0,6
Width= 8 m
Radius= 11 m
15 m
N3
Depth= 1,3
Width= 10 m
Radius= 21 m
15 m
N4
Depth= 0,6
Width= 6 m
Radius= 13 m
15 m
S1
Depth= 0,5
Width= 11 m
Radius= 15 m
15 m
S2
Depth= 1,4
Width= 6 m
Radius= 6 m
15 m
S3
Depth= 1,2
Width= 9 m
Radius= 11 m
15 m
S4
Depth= 0,9
Width= 2 m
Radius= 8 m
15 m
N

Figure 3 Satellite images (from Google™Earth) showing the study meander bends in the Northern (N1, N2, N3, and N4) and Southern (S1, S2, S3, and S4) Lagoon. Dots indicate the position of the recovered cores in each meander.

The study case bends are 2 – 11 m wide and 0.5 –1.6 m deep (Fig 3), and cut through salt marshes colonized by a dense halophytic vegetation species such as *Limonium narbonense*, *Spartina maritima*, *Sarcocornia fruticosa*, *Juncus maritimus*, and *Salicornia veneta*. All the study channel bends are still active, made exception for that at site N4 (Fig 3), which is now completely filled following a cutoff occurred during the 1950s (D'Alpaos et al., 2017). None of the active channels is completely dried out at the lowest tides, and point bar top can be covered by few decimeters of water at the highest tides. Meanders at sites N2 and S2 show a "simple asymmetric" (*sensu* Brice, 1974) planform geometry, whereas all the other channels can be labelled as "simple symmetric" (*sensu* Brice, 1974). The radius of curvature of the bends ranges between 6 and 21 m (Fig 3).

3. METHODS AND TERMINOLOGY

A total of 50 cores were recovered along axial transects of the study bends. Each transect extended from the channel thalweg to the line connecting inflection points of the bend (Fig 3). The position and elevation of the cores was determined using differential GPS TOPCON GR-3 receivers – dual frequency (L1/L2) and dual-constellation (NavStar/Glonass) with integrated Tx/Rx UHF radio. Cores were up to 3 m deep and were recovered using an Eijkelkamp hand auger, through a gouge sampler with a length of 1 m and a diameter of 30 mm, which prevented sediment compaction. PVC liners were used to keep the cores humid, which were successively cut longitudinally, photographed and logged. Sedimentological analyses were carried out on the study cores following the basic principles of facies analyses. Identification of different types of deposits (Fig 5 and 6) was based on the integration between core location and related sedimentary features, including sediment grain size and color, presence of sedimentary structures, vertical grain-size trends, degree of bioturbation and occurrence of plant and/or shell remains. Correlation among cores allowed to disclose 2D point bar sections along the bend axis (Fig 7 and 8).

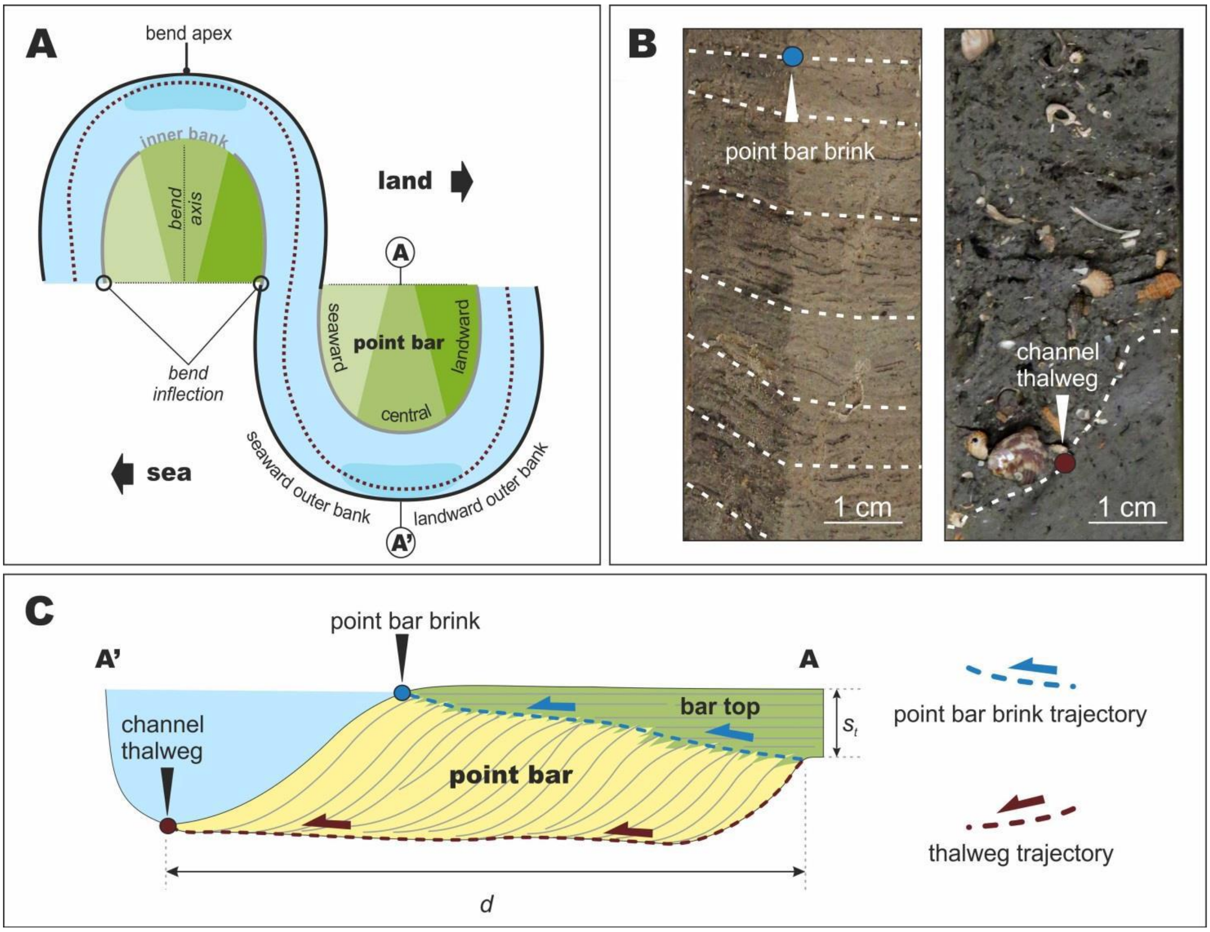

Figure 4 Terminology used in the present work. (A) Key terms used to define different elements of tidal meander bends. (B) Examples of point bar brink (left) and channel thalweg (right) deposits in sedimentary cores. (C) Tidal point bar architecture and definition of point bar brink and thalweg trajectories. st: maximum thickness of bar top, salt-marsh deposits accumulated during bar migration. d: distance covered by the lateral shift of the channel.

Terminology used in the present work is reported in figure 4, and follows that used for fluvial point bars (cf. Ielpi and Ghinassi, 2014), although some modifications have been introduced due to the bidirectional nature of tidal currents (e.g. seaward/landward instead of downstream/upstream). The point bar brink is defined here as the bar rim (Fig 1A and 4C), characterized by a break in the angle of deposition from the flat bar top deposits to the inclined bar slope. Accordingly, in cores, the point bar brink was pointed out where lamination changed from horizontal (i.e. bar top deposits) to inclined (i.e. bar slope deposits). This change in inclination occurs within an interval spanning between 5 and 10 cm in thickness (Fig 4B), which represents the uncertainty for detecting the brink position in the study deposits. The channel thalweg is defined as the deepest part of the active channel (Fig 1A and 4C). In cores, it corresponds to the surface flooring channel lag deposits and can be precisely located (Fig 4B).

Minimum and maximum lateral migration rates (ζ_{min}, ζ_{max}, *respectively*) of each bend have been approximately estimated on the basis of the ratio between the distance covered by the lateral shift of the channel (*d* in figure 4C) and the minimum and maximum estimated time span over which migration occurred (Δt_{min} and Δt_{max}). The latter have been determined as $\Delta t_{min}=s_t/s_{a,min}$ *and* $\Delta t_{max}=s_t/s_{a,max}$, where s_t is the maximum thickness of bar top salt-marsh deposits accumulated during bar migration (Fig 4C) and $s_{a,min}$ and $s_{a,max}$ are the minimum and maximum vertical accretion rates of salt marshes reported in literature for the study area (Bellucci et al., 2007; Roner et al., 2017).

4. RESULTS

4.1 Study deposits

4.1.1 Substrate deposits

These deposits represent the lowermost stratigraphic unit of each study case, and are radically different in the Northern and Southern Venice Lagoon.

In the Northern Lagoon, they consist of an alternation between sandy and muddy layers. The sandy layers, that can locally exceed 1 m in thickness, consist of well-sorted dark gray sand, medium to very fine in grain size, with abundant shells, shell fragments and plant debris (Fig 5B). Sandy deposits can locally contain millimetric muddy laminae. The muddy layers consist of dark, organic-rich mud with scattered shells and plant fragments, and are up to 10 cm thick (Fig 5A). Bioturbation is common in both the sandy and muddy layers, and prevents detection of sedimentary structures. Substrate deposits of the Northern Lagoon are interpreted to be formed in a tidal flat/subtidal platform environment. Sandy deposits were likely originated during wind-induced storm events, when wave winnowing entrained fine-grained sediments and sand concentrated on the lagoon floor (Carniello et al., 2009). Muddy deposits were settled down from suspension during the waning stage of storm events.

In the Southern Lagoon, substrate deposits consist of peat with abundant fragments of reeds (Fig 5D). In some of the cores from sites S2 and S3, a dark-gray mud interval with sparse reed fragments (Fig 5C) occurs on top of peat deposits. Peat consists of comminuted dark brown to black plant debris with a minimum amount of dispersed mud. The presence of peat deposits and abundant reeds is consistent with a wetland setting with freshwater input (Bondesan and Meneghel, 2004; Tosi et al., 2007). The mud on top of peat deposits could be related to local protected ponds, where vegetation cannot grow and mud can settled down (Roner et al., 2016; Silvestri et al., 2005). Although peat is widespread in the Southern Lagoon (Roner et al., 2017), substrate deposits at site S4 (Fig 2) consist of an alternation between mud and sand similar to that occurring in the Northern Lagoon.

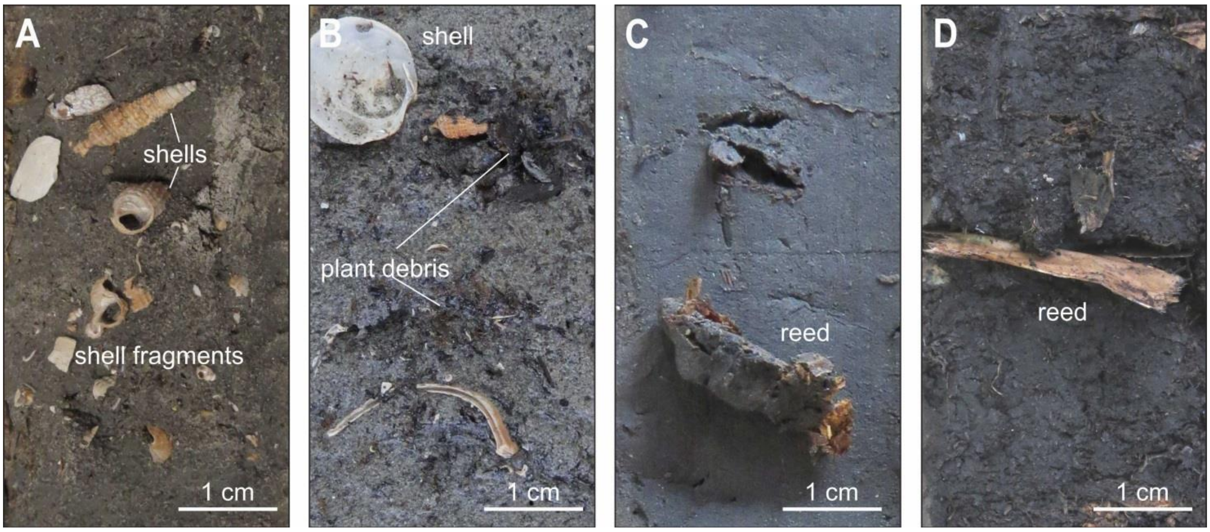

Figure 5 Substrate deposits of the Northern (A and B) and Southern (C and D) Lagoon. (A) Organic-rich mud with shells and plant fragments; (B) Dark-gray sand, medium to very fine in grain size, with abundant shells, shell fragments and plant debris. (C) dark-gray mud with scattered reed fragments; (D) Peat with abundant fragments of reeds.

4.1.2 Point bar and channel lag deposits

These deposits are up to 2.25 m thick, and show a lateral extent of 10-20 m, and 3-15 m for the Northern and Southern sites, respectively (Fig 9). These deposits pinch out toward both the terminations of all the study transects (Fig 8). They are erosively-based and grade upward into salt marsh or channel-fill deposits. The basal erosional surface is draped by a shell-rich, 5-20 cm thick massive layer (Fig 6 A.7 and B.5), which consists of fine to medium sand and of silt to fine sand in the Northern and Southern sites, respectively. Shells are commonly fragmented and include both gastropods (e.g. *Bittium scabrum, Tritia neritea, Gibbula* sp.) and bivalves (e.g. *Loripes orbiculatus, Acanthocardia tubercolata, Scrobicularia plana*). Plant debris and pebble-sized, rounded mud clasts are also common (Fig 6 A.6).

The shell-rich layer is covered by clinostratified deposits, which are up to 2.2 m thick and show an overall fining-upward grain size trend (Fig 6 A and B). Clinostratified deposits consist of two intervals. The lower interval is made of fine sand to silt-rich mud with scattered shell fragments and mud clasts. These deposits are mainly massive (Fig 6 A.4), although a local inclined lamination is slightly visible (Fig 6 B.3). Bioturbation is really common and often prevent the identification of primary bedding (Fig 6 A.5). The upper interval ranges in grain size between sandy silt and mud and shows a clear inclined heterolithic stratification, with laminae dipping channelward between 5° to 25° (Fig 6 A, A.3, B and B.2). Laminae consist of well-sorted very-fine to fine sand (Fig 6 A.3) or comminuted plant debris (Fig 6 B.2), which are more common in the Northern and Southern sites, respectively. Inclination of laminae decreases moving upward in the clinostratified deposits, and becomes insignificant at the boundary with the overlying salt-marsh deposits (Fig 6 A, A.3 and B).

The shell-rich basal layer and the overlying clinostratified silty sand are interpreted as channel lag and point bar deposits, respectively. Channel lag deposits accumulated in the deepest part of the channel, where the coarser sediments and shell fragments concentrate, as finer grains are entrained by currents (Terwindt, 1988). Shelly assemblages consist of mainly marine and subordinately brackish molluscan species that roughly reflect the benthic fauna currently inhabiting mud and sandy substrates of the Venice Lagoon. Pebble-sized mud clasts are the product of fragmentation of blocks collapsed from the channel banks (Terwindt, 1988). Clinostratified bar deposits accumulated as a consequence of lateral shift of the channel, and their fining-upward grain size trend, reflect the overall decrease of the bottom shear stress moving from channel thalweg to bar top in the axial zone of a meander bend (Dietrich et al., 1979; Dietrich and Smith, 1984; Frothingham and

Rhoads, 2003; Hooke, 1975). In the lower bar deposits (i.e. lower part of clinostratified sediments), intense bioturbation, and related paucity of sedimentary structures, is consistent with the permanent presence of water on this part of the bar. In the upper bar deposits (i.e. upper part of clinostratified sediments), the dominance of mud points out to prevalence of fallout processes, which were probably dominant during prolonged slack water periods or after storm events (Carniello et al., 2011). Inclined sandy laminae of the upper bar were produced during storms at high tides, when both salt marshes and bar tops were winnowed by waves (Carniello et al., 2011; Choi and Jo, 2015; Fruergaard et al., 2011; Green and Coco, 2007). The decrease in the inclination of laminae reflects the progressive upward flattening of bar slope and heralds the transition into overlying salt-marsh deposits.

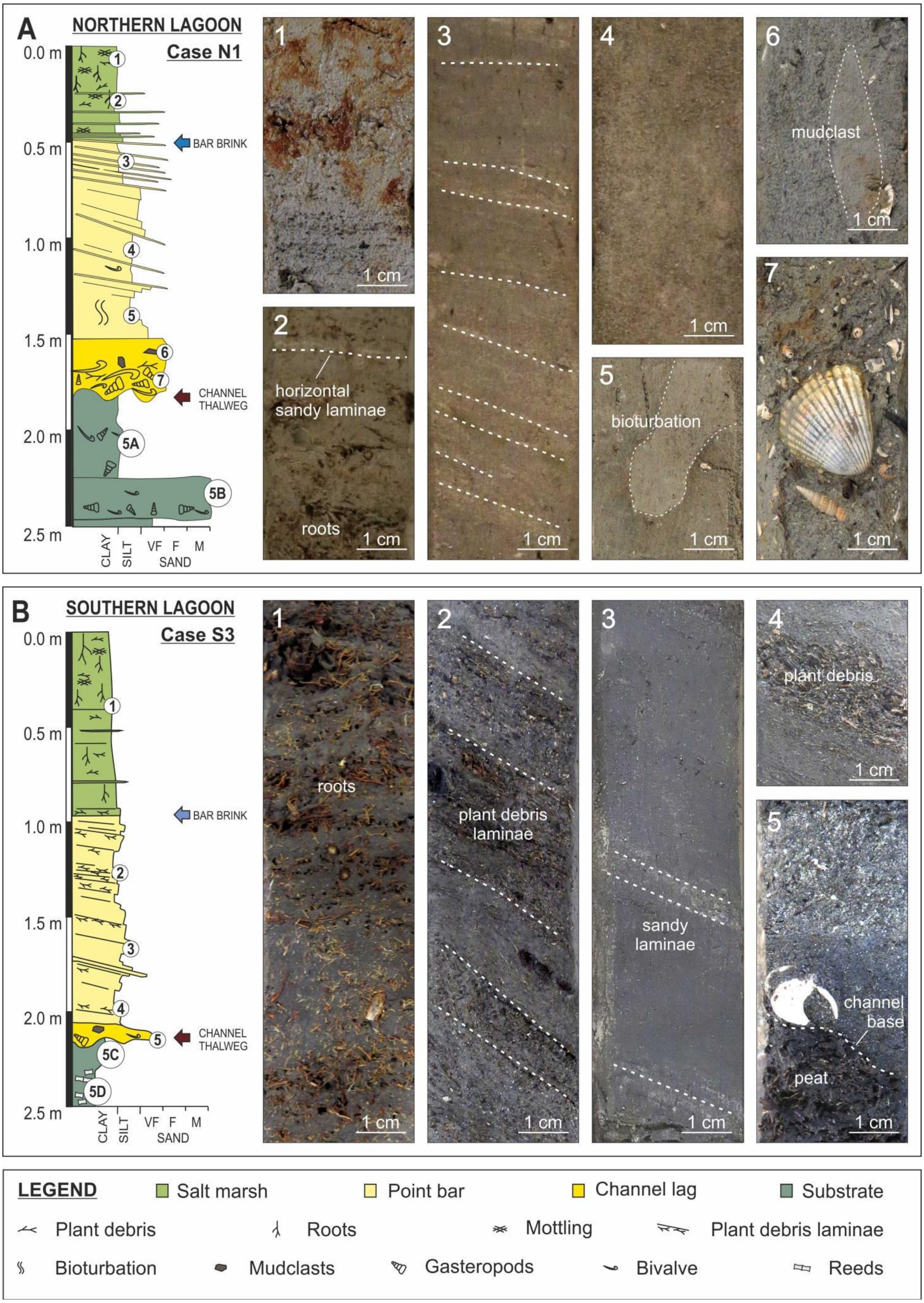

Figure 6 Point bar deposits from Northern and Southern study sites. (A) Northern Case. Example from site N1; (A.1) Oxidized salt-marsh mud; (A.2) Salt-marsh mud with horizontal sandy laminae and roots; (A.3)

Heterolithic bar deposits consisting of silt with inclined sandy laminae. Note the upward decrease in dip angle of sandy laminae; (A.4) and (A.5) Structureless sand and bioturbation in the lower part of the point bar; (A.6) Pebble-sized mudclast in massive channel-lag sand; (A.7) Shell-rich channel-lag sand; (B) Southern Case. Example from site S3; (B.1) Salt-marsh mud deposits with roots; (B.2), (B.3) and (B.4) Silty to muddy bar deposits with a variable amount of inclined plant debris and sandy laminae; (B.5) Massive channel-lag sand with shells and shells fragments, flooring the channel base.

4.1.3 Salt marsh deposits

Salt-marsh sediments commonly cover point bar bodies, but they can also overlay substrate deposits. Salt-marsh deposits consist of brownish, oxidized mud with 1-3 mm thick horizontal well-sorted sandy laminae (Fig 6 A.1, A.2 and B.1). In situ roots, wood fragments and bioturbation are common. Along each transect, the thickness of these deposits decreases toward the channel (Fig 8). Maximum thicknesses of salt marsh deposits is 0.7 and 2 m in the Northern and Southern sites, respectively (s_t in figure 9).

Salt-marsh deposits accumulate in the upper part of the intertidal zone, where subaerial exposure is frequent (Silvestri et al., 2005). This is in agreement with widespread oxidation and occurrence of abundant roots. These deposits are mainly accreted through mud settling and organic matter accumulation (Allen, 2000; Mudd et al., 2010; Roner et al., 2016). Muddy sediments are deposited by fallout during high water slacks, at the transition between flood and ebb tide. Sorting of sand forming thin laminae suggests their formation during storm events, when salt-marsh surface was flooded and wave-winnowing suspended mud particles and concentrated coarser sediments (Choi and Jo, 2015).

4.1.4 Channel-fill deposits

These deposits occur only at sites N2, N4 and S1 (Fig 8), are up to 1.5 m thick and overlie point-bar and channel-lag sediments. At the abandoned channel bend of site N4 they are thick as the adjacent point bar, whereas at sites N2 and S1 they are thinner than the bar. These deposits consist of dark gray, massive mud with dispersed bivalves in life position. At sites N4 and S1 (Fig 8), the transition between these deposits and underlying point bar sand is transitional.

These muddy deposits settled down from suspension, silting up channels affected by a progressive decrease in water discharge. In case of site N4, deactivation of the channel followed a neck cutoff, which allowed the whole channel to be filled with mud (D'Alpaos et al., 2017). At sites N2 and S1, the increase of fallout processes can be ascribed to a general decrease in the discharge shaping the tidal network in the area, and the gradual transition from underlying bar deposits points out to a progressive deactivation of the channel (cf. Toonen et al., 2012).

4.2 Point bar brink and channel thalweg trajectories

The stratigraphic relationship between different sedimentary facies marked location of point bar brink (i.e. transition between point-bar and salt-marsh deposits) and thalweg (i.e. base of channel lag deposits) zone in all the study cores. Correlation between adjacent cores depicted the point bar brink and channel thalweg trajectories, which were generated during lateral shift of the channel and accumulation of related point-bar bodies (Fig 7). Brink and thalweg trajectories start from a shared point (i.e. "nucleation point" in figure 7) and follow specific paths, which are summarized in figure 8, where the vertical scale has been doubled in order to emphasize different trends.

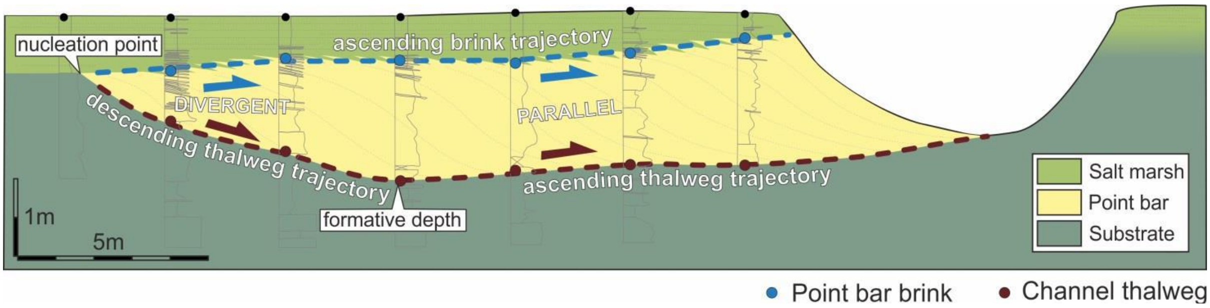

Figure 7 Correlation between cores along the axis of point bar N1. Bar brink and channel thalweg trajectories are highlighted.

All the reconstructed bar brink trajectories show an ascending pattern (Fig 8), although some of them show low steepness (less than 2°) and can be considered sub-horizontal. In sites located in the Northern Lagoon, the trajectories appear to be gentle and linear, with a constant slope ranging between 0.3 and 1.7° (Fig 8 N1-N4). In the Southern Lagoon, a linear and gentle (2.9°) trajectory occurs only at site S4, whereas sites S1 – S3 are characterized by curve and steep trajectories. At sites S2 and S3 (Fig 8), the trajectories show a concave-upward profile, with a slope inclination that changes from sub-horizontal to ca. 41.5° and 9.4°, respectively (Fig 8). At site S1 the brink trajectory defines a convex-upward profile, with the slope decreasing from 16.2° to 6.6°.

The thalweg trajectories appear to be more complex and result from the combination of descending, horizontal and ascending shifts. In all the study cases (Fig 8), with the exceptions of the site N2 (where nucleation point has not been detected), the thalweg trajectories show an initial downward shift. The steepness of this descending segment varies from 6.3° to 31.6° and shows a linear or faintly concave-upward geometry (Fig 8). After this first descending reach, the following portion of the trajectories shows either gentle (N1 – N4) or steep (S1 – S4) slopes. In the Northern sites, these trajectories are commonly sub-horizontal with slightly ascending (N1) or descending (N2-N3) shifts. In the Southern cases, they rise up with inclination ranging between 4.8° and 23.3° (Fig 8). None of the ascending reach show convex- or concave-upward geometries.

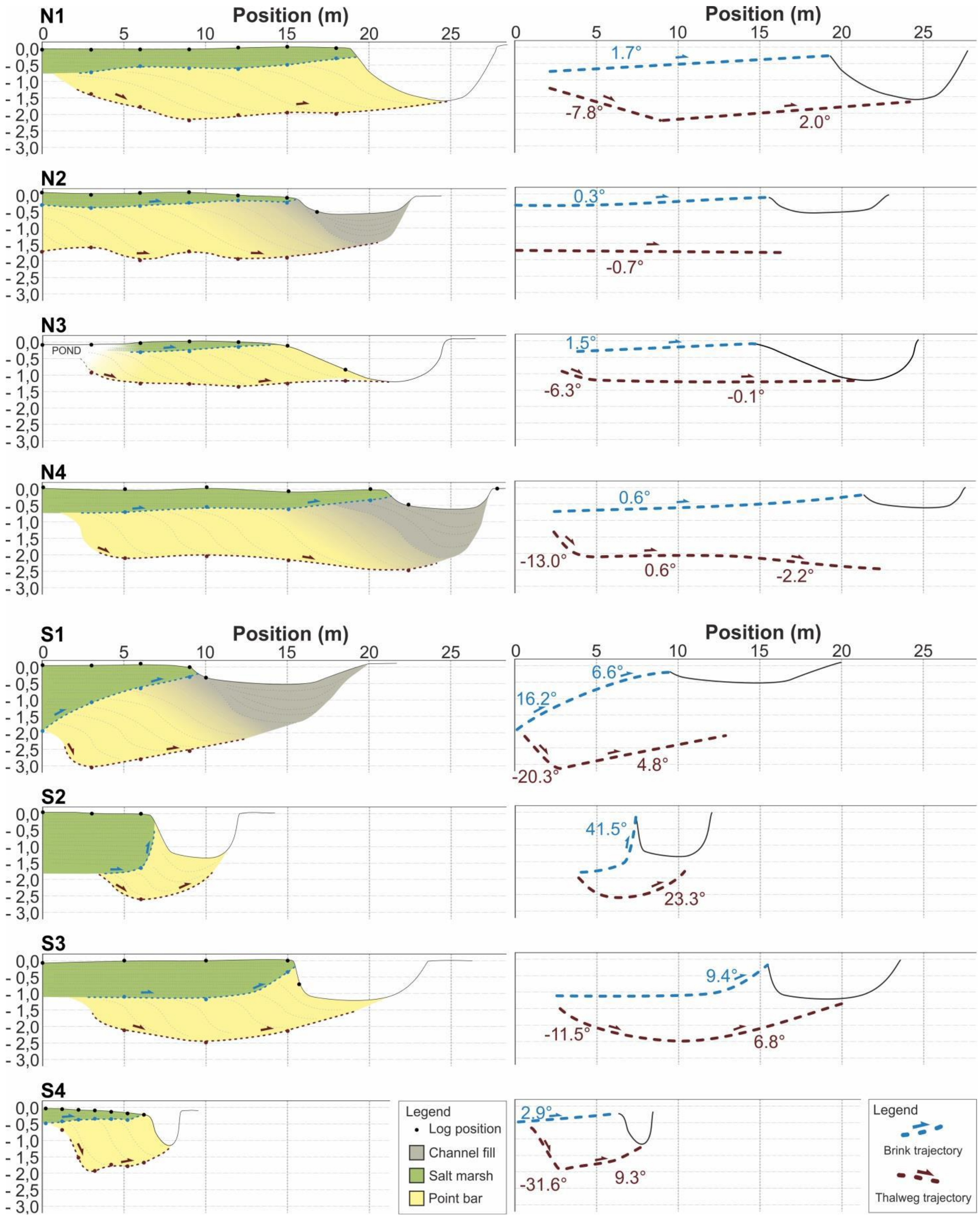

Figure 8 Point bar sections of the northern (N1 – N4) and southern (S1 – S4) study cases. Point bar brink and thalweg trajectories are marked with light blue and red dotted lines, respectively. Slopes of bar brink and channel thalweg trajectories are shown on the right side of the figure. Vertical exaggeration x2.

Different combinations of bar brink and thalweg trajectories occur at different sites (Fig 11), although all the study cases share an early stage where brink and thalweg trajectories diverge (Fig 7 and 8), causing an increase of point bar thickness. This pattern has not been tested at site N2, since deposits of the early channel evolution were not cored (Fig 8). This early stage of divergence occurs over distances spanning between 1 and 7 m, and the angle of divergence ranges between 7.8° (N3) and 36.5° (S1). After the stage of divergence, different patterns of brink and thalweg trajectories are combined. At Northern sites (N1 – N3), gently ascending brink trajectories are combined with similar thalweg trajectories. At site N4, after an initial similar pattern (ascending brink and thalweg) a phase of divergence of brink and thalweg trajectories is recorded. At Southern sites, the stage of divergence is also followed by a stage in which brink and thalweg trajectories show a similar ascending pattern (S1 – S3). Site S4 does not show this trend and, after the stage of divergence, the thalweg trajectory rises converging toward the corresponding brink trajectory.

4.3 Lateral migration rates

The lateral migration rate of each bend has been estimated through a comparison between the maximum thickness of salt-marsh deposits overlying different bars and aggradation rates documented in the study areas (Bellucci et al., 2007; Roner et al., 2017). Figure 9 shows that maximum migration rates do not exceeds 0.2 m/yr (N2). Minimum migration rates obtained for the Northern and Southern sites are in the range of 0.02-0.04 m/yr and 0.002-0.01 m/yr, respectively; maximum migration rates span between 0.11-0.19 m/yr in the Northern meanders, and between 0.02-0.16 m/yr in the Southern meanders. These values are consistent with other studies carried out for meandering channels of the Venice Lagoon (Brivio et al., 2016; D'Alpaos et al., 2017; Donnici et al., 2017; Finotello et al., 2018; Ghinassi et al., 2018a; McClennen and Housley, 2006) and in other microtidal environments worldwide (Gabet, 1998; Garofalo, 1980).

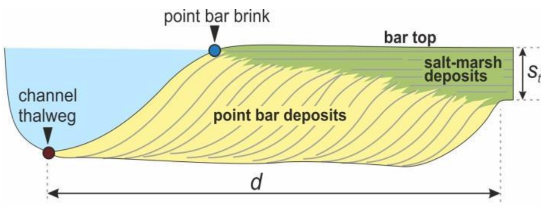

ACCRETION RATE ($s_{a,min}$ - $s_{a,max}$)

Northern Venice Lagoon (Bellucci et al., 2007): **0.1 - 0.5 cm/yr**

Southern Venice Lagoon (Roner et al., 2017): **0.1 - 1.2 cm/yr**

	site	s_t (m)	d (m)	ζ_{min} (m/yr)	ζ_{max} (m/yr)
NORTHERN CASES	N1	0.70	15	0.02	0.11
	N2	0.40	15	0.04	0.19
	N3	0.30	10	0.03	0.16
	N4	0.70	20	0.03	0.14
SOUTHERN CASES	S1	2.00	9	0.005	0.05
	S2	1.65	3	0.002	0.02
	S3	1.10	15	0.01	0.16
	S4	0.47	6	0.01	0.15

Migration Rate $(\zeta) = d / \Delta t = (d * s_a) / s_t$

$\Delta t = s_t / s_a$

Figure 9 Estimation of minimum (ζmin) and maximum (ζmax) lateral migration rates of the different meanders considering maximum (sa,max) and minimum (sa,min) salt marsh accretion rates reported in the literature.

5. DISCUSSION

Trajectory analysis has been applied here at the point-bar scale, showing the migration patterns of the point bar brink and the channel thalweg along axial cross sections of different tidal bends. Trajectories are labelled as ascending, descending and horizontal (Fig 10). Ascending and descending trajectories are distinguished in linear and non-linear (Fig 10). While linear trajectories document a constant ratio between vertical and lateral shift rates (d (v/ζ) /dt = 0), non-linear trajectories, which can be concave- or convex-upward, document temporal changes in the ratio between vertical and lateral shift rates (d (v/ζ) /dt ≠ 0).

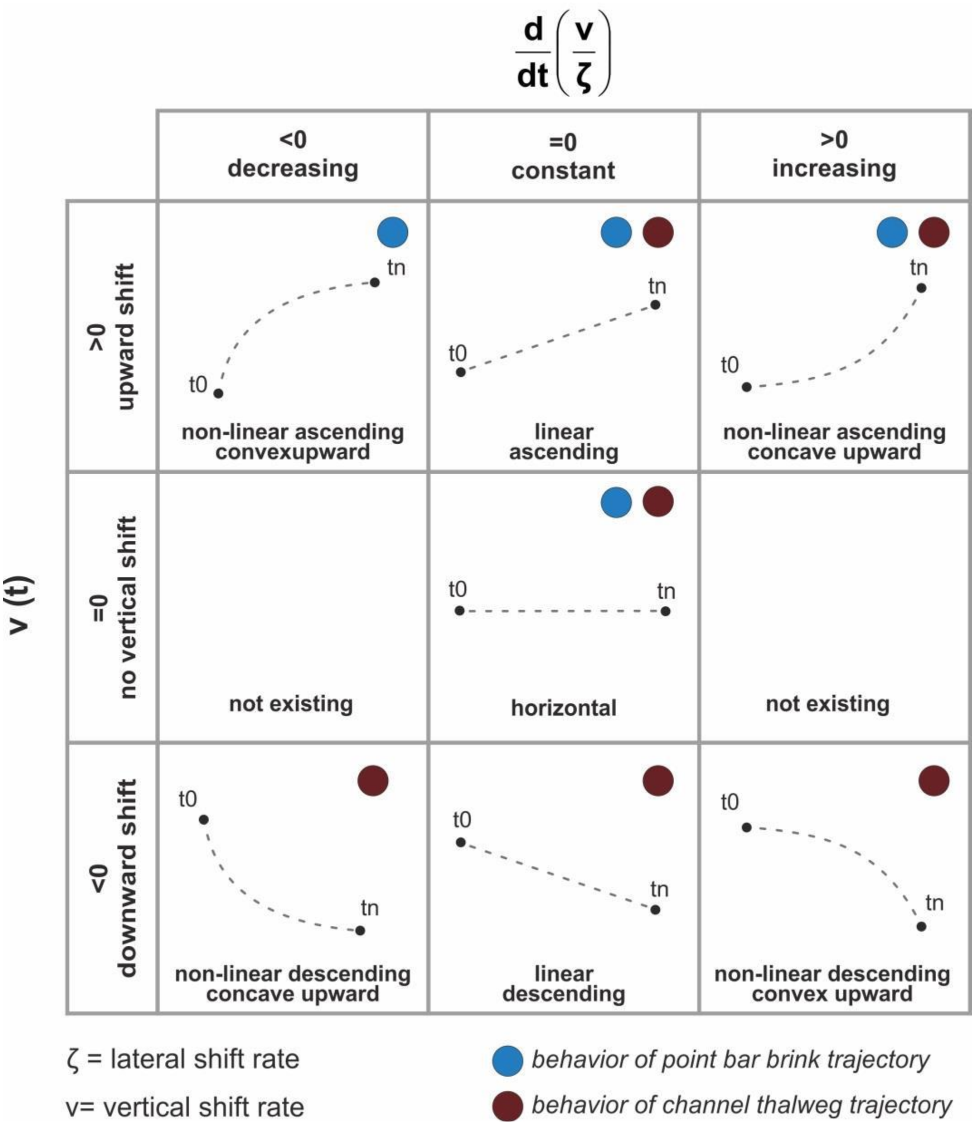

Figure 10 Different types of point bar brink and channel thalweg trajectories.

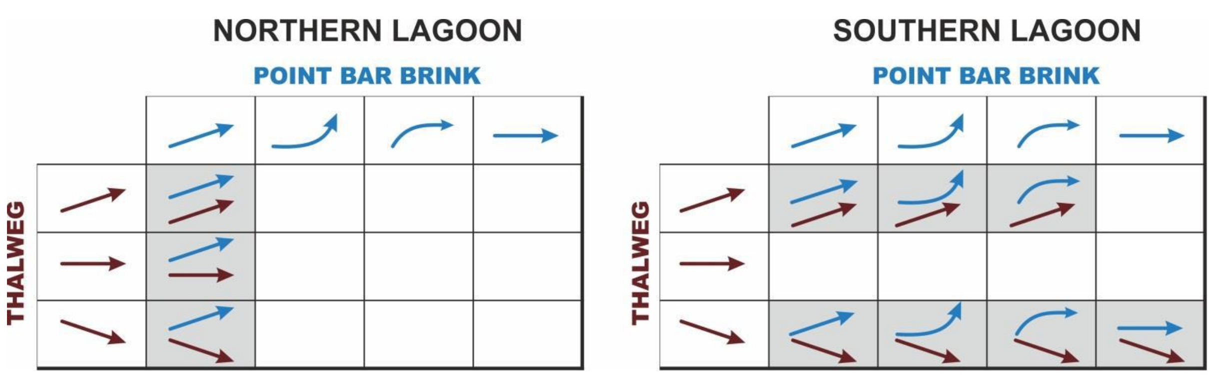

Figure 11 Combinations of point bar brink and channel thalweg trajectories registered in northern and southern cases.

5.1 Point bar brink trajectories

Ascending point bar brink trajectories point out that the lateral shift of the brink was influenced by aggradation of surrounding salt-marshes, which kept pace with the progressive sea-level rise by accreting both inorganic and organic sediments (D'Alpaos et al., 2007; Morris et al., 2002; Mudd et al., 2010). Steepness of brink trajectories reflects a different ratio between vertical accretion and lateral migration, and, where lateral shift rate dominates over that of vertical aggradation, the brink trajectories will appear sub-horizontal (i.e. less than 2°). Conversely, where vertical aggradation is higher, it forces the brink to define steep trajectories (i.e. up to 41.5°). The remarkable difference in the flat and steep trajectories observed in the Northern and Southern Lagoon, respectively, can hardly be ascribed to the slightly difference between aggradation rates of these two areas (Bellucci et al., 2007; Roner et al., 2017). Therefore, a further constraint is considered to be responsible of this remarkable difference, namely the nature of substrate deposits hosting different bars. Peat deposits, like those hosting S1-S3 bars, are the most compressible of all natural soils (Allen, 1999) and their compaction leads to a substantial increase of local subsidence (Long et al., 2006; Rajchl and Uličný, 2005; Törnqvist et al., 2008; van Asselen, 2011; van Asselen et al., 2010). Peat deposits can be compacted up to 43% within few centuries (van Asselen et al., 2010), with compaction rates that can exceed 10 mm/yr, on decadal to centenary timescales (Törnqvist et al., 2008). The dominant factors influencing peat compaction are the organic matter content and the sediment loading of overlying deposits (Elliott, 1985; van Asselen, 2011; van Asselen et al., 2010). The peat of the Southern Lagoon was progressively compacted by the increasing sediment load due to the growth of the overlying point bars, with a significant increase of local subsidence and related aggradation (Fig 12). The lack of a steep brink trajectory at bar S4, which covers a sandy substrate, supports this hypothesis. Progressive compaction of peat substrate is also consistent with the occurrence of non-linear and concave-upward trajectories (sites S2 and S3; Fig 8), which point out a progressive increase of the ratio between vertical and lateral shift rate. This increase was due to intensification of local subsidence/aggradation triggered by loading exerted by the growing of bar deposits over peat deposits. The non-linear convex-upward trajectory at site S1 documents a progressive decrease in the ratio between vertical and lateral shift rate. Progressive flattening of this trajectory points out to a relative increase in lateral channel shift, which would be caused by the occurrence of erodible deposits (e.g. sand) along the outer bank of the channel (cf. Ghinassi et al., 2016; Smith et al., 2009). Linear and gently-sloping trajectories of the Northern sites indicate that the ratio between vertical and lateral shift rate remained constant during lateral shift of the channel, and that rate of lateral migration dominated over that of vertical shift. The presence of a sand-prone substrate in the Northern Lagoon nullifies the effects of local substrate compaction, hindering the development of curvilinear trajectories.

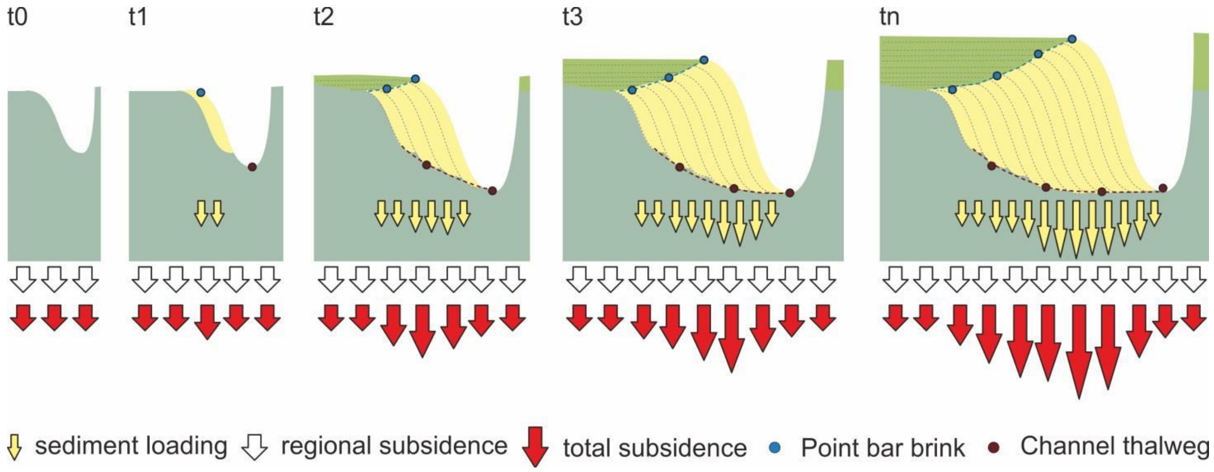

Figure 12 Diagram illustrating the influence of substrate compaction on developing of bar brink and channel thalweg trajectories. The progressive increase of bar sediment loading on the peaty substrate, causes a local increase in subsidence/accretion, which are documented by development of steep brink trajectories.

5.2 Channel thalweg trajectories

Channel thalweg trajectories include ascending, descending and horizontal trends, indicating that the channel base shifted laterally under aggradational, degradational and stable conditions, respectively. The lack of clear convex- or concave-upward profile of ascending and descending trajectories could point to a stable ratio between lateral and vertical shift rates, although the erosive (i.e. irregular) nature of the channel basal surface could prevent a clear detection of these trends.

The descending thalweg trajectories which characterize the early part of all the study trajectories, document the establishment of the channels, which shift laterally and cut down into the substrate in order to reach a cross sectional depth that is in equilibrium with the local, formative tidal prism. The formative depth in the bend axial zone is function of the channel discharge and bend geometry. Channel discharge is related to the tidal watershed area, and can vary over temporal scales of decades to centuries as consequence of changes in the tidal prism, watershed area (e.g. due to channel piracies and/or meander cutoff) and channel network evolution (Allen, 2000; D'Alpaos et al., 2005; Dalrymple et al., 1991; Garofalo, 1980; Lanzoni and Seminara, 2002; Stefanon et al., 2012). Bend geometry can influence the capability of the channel to cut through its substrate (Crosato, 2009; Hooke, 1984; Hudson and Kesel, 2000; Lagasse et al., 2004; Nanson and Hickin, 1986). Specifically, a progressive increase in bend sinuosity enhances the erosive power of the secondary helical flow, causing a progressive deepening of the pool in the axial zone of the bend (Willis and Tang, 2010). The slope of descending thalweg trajectories indicates the rate of channel incision, which reflects the amount of time required to reach the equilibrium depth.

The thalweg trajectories, which characterize the evolution of the meander after the achievement of the formative depth, show either sub-horizontal (N1 – N4) or steep (S1 – S4) ascending patterns. Sub horizontal thalweg trajectories (inclination < 2°) point out that the channel mainly shifted laterally with a minor influence of aggradational or degradational processes. Rising thalweg trajectories indicate that the channel shifted laterally under aggradational conditions, and, as for bar brink trajectories, gently- and steeply-rising trajectories are associated with a low and high values of the ratio between vertical and lateral shift rate, respectively. In-channel aggradation can either occur when its transport capability decreases, as in consequence of avulsion or cutoff (Toonen et al., 2012), or when, under aggradational and short-term dynamic equilibrium conditions (*sensu* Allen, 2000), sediments are stored in the channel in order to maintain a constant equilibrium depth. The first scenario is documented at sites N2, N4 and S1 (Fig 8) and implies the progressive decrease of channel cross-sectional area trough deposition of fine-grained sediments on the channel floor. The similarity between depth of active channels (N1, N3 and S2 – S4) and thickness of the associated bar indicate that they migrated depositing sediments at their base in order to keep the equilibrium with the surrounding environment.

5.3 Brink and thalweg trajectory combinations

The study sites document an early stage where brink and thalweg trajectories show an ascending and descending trends, respectively. This stage, named “formative phase” in figure 13, documents the onset of bar depositions and the achievement of the channel depth equilibrium. The angle between brink and thalweg trajectory controls the increase in point bar thickness, and is higher where channels cut rapidly into highly-aggrading marshes. Minor modifications to this process are represented by changes in climbing angle of the brink trajectory, which can be triggered by changes in ratio between vertical and lateral shift rate of the channel.

Once the equilibrium depth is reached, six of eight study channels show that thalweg and brink trajectories move following an almost parallel pathway (“equilibrium phase” in figure 13). It arises that, once the channel reached its equilibrium depth, this was kept constant shifting the thalweg in parallel with the bar brink zone. Minor variations from this overall behavior are documented at sites N4 and S4. Thalweg trajectory at site N4 slightly cuts down before the onset of the abandonment stage (Fig 8). This downward shift would be consistent either with an increase in water discharge, possibly due to a piracy in the upstream reaches of the tidal network, or with an increase in channel sinuosity due to adjustment of its planform shape. Differently, the rising thalweg trajectory at site S4 suggests that after reaching its formative depth, the channel decreased its discharge, possibly as consequence of changes in channel network structure.

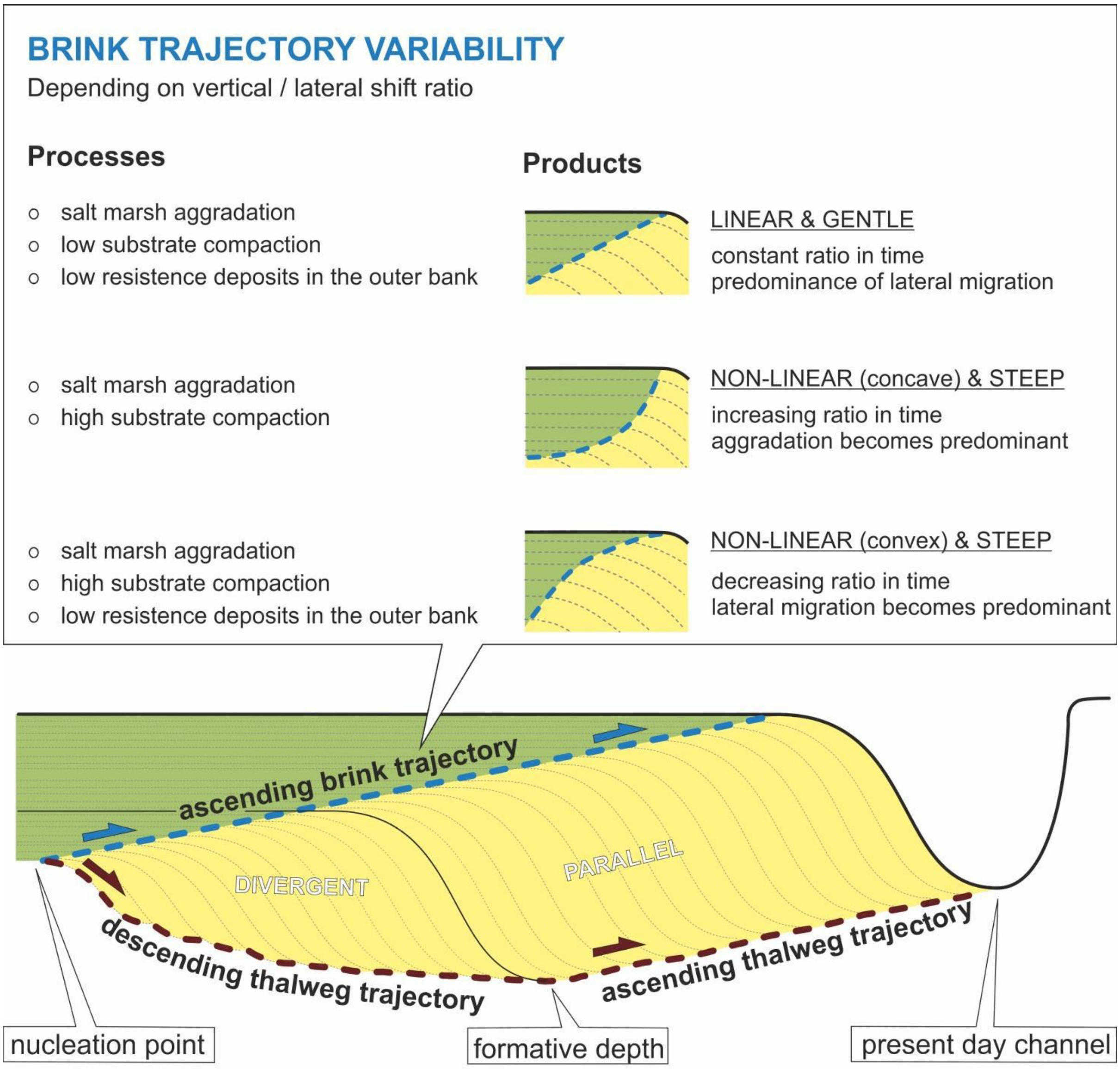

FORMATIVE PHASE	EQUILIBRIUM PHASE
DIVERGENT brink and thalweg trajectories	**PARALLEL** brink and thalweg trajectories
Growth of the channel toward its equilibrium	The channel keeps the equilibrium cross section
Increase in point bar thickness	Constant point bar thickness

Figure 13 Summary of the main architectural features associated with development and combination of different point bar brink and channel thalweg trajectories.

6. CONCLUSIONS

The concept of trajectories analysis has been applied at the point bar scale in order to improve our understanding of the behavior of tidal point bars in micro-tidal and highly aggradational landscapes.

The main conclusions, as highlighted in figure 13, can be summarized as follows:

i) Bar brink trajectories are all ascending and show linear or non-linear trends whether the ratio between vertical and lateral shift rate is constant or not through time. When this ratio increases or decreases through time, non-linear trajectories show a concave- or convex-upward profile, respectively (Fig 10). The different shapes and steepness of these trajectories suggest that the bar brinks register different aggradational conditions while shifting laterally.

ii) The local increase in subsidence, due to bar loading on a soft (i.e. peaty) substrate can be a key factor for the development of steep brink trajectories. In particular, our results suggest that the differential compaction of sandy and peaty substrates plays a significant role in the creation of local accommodation, which controls the steepness of the trajectory.

iii) Thalweg trajectories can be both ascending and descending. The different inclination of the descending portion of the thalweg trajectory can be ascribed to the incision rate of the channel while shifting laterally. This is influenced by local tidal prism, bend geometry and evolution of the channel network. Ascending thalweg trajectories suggest that the channel shift laterally under aggradational conditions.

iv) The combination of brink and thalweg trajectories reveals the variation of point bar thickness during its evolution and allows one to differentiate and early formative phase followed by a late equilibrium phase. During the formative phase, the two trajectories diverge from one another because of the growth of the channel toward its equilibrium depth (formative depth). In the following equilibrium phase, the two trajectories shift in parallel, allowing the channel to keep its equilibrium depth. Variations to this evolution model can be triggered by modification of channel discharge, possibly triggered by piracy events and channel network evolution.

ACKNOWLEDGEMENTS

This work was supported by the following research projects: i) SID2016 project of Padova University titled “From channels to rock record: morphodynamic evolution of tidal meanders and related sedimentary products” (prot. BIRD168939); ii) SHELL International Exploration and Production project titled “Tidal vs. tidally-influenced fluvial point bars: facies distribution and implications for reservoirs production development”, and iii) HYDROSEM project (Progetto di Eccellenza CARIPARO 2017).

Declarations of interest: none

REFERENCES

Allen, J.R.L., 2000. Morphodynamics of Holocene salt marshes: a review sketch from the Atlantic and Southern North Sea coasts of Europe. Quat. Sci. Rev. 19, 1155–1231.

Allen, J.R.L., 1999. Geological impacts on coastal wetland landscapes: Some general effects of sediment autocompaction in the Holocene of northwest Europe. The Holocene 9, 1–12. https://doi.org/10.1191/095968399674929672

Amorosi, A., Fontana, A., Antonioli, F., Primon, S., Bondesan, A., 2008. Post-LGM sedimentation and Holocene shoreline evolution in the NW Adriatic coastal area.

GeoActa 7, 41–67.
Barwis, J.H., 1978. Sedimentology of some South Carolina tidal-creek point bars, and a comparison with thier fluvial counterparts, in: Miall, A.D. (Ed.), Fluvial Sedimentology. Canadian Society of Petroleum Geologists Memoir 5, pp. 129–160.
Beeson, C.E., Doyle, P.F., 1995. Comparison of bank erosion at vegetated and non-vegetated channel bends. Water Resour. Bull. 31, 983–990.
Bellucci, L.G., Frignani, M., Cochran, J.K., Albertazzi, S., Zaggia, L., Cecconi, G., Hopkins, H., 2007. 210Pb and 137Cs as chronometers for salt marsh accretion in the Venice Lagoon - links to flooding frequency and climate change. J. Environ. Radioact. 97, 85–102. https://doi.org/10.1016/j.jenvrad.2007.03.005
Boaga, J., Ghinassi, M., D'Alpaos, A., Deidda, G.P., Rodriguez, G., Cassiani, G., 2018. Geophysical investigations unravel the vestiges of ancient meandering channels and their dynamics in tidal landscapes. Sci. Rep. 8, 1–8. https://doi.org/10.1038/s41598-018-20061-5
Bondesan, A., Meneghel, M., 2004. Geomorfologia della provincia di Venezia. Note illustrative della carta geomorfologica della provincia di Venezia.
Brice, J.C., 1974. Evolution of Meander Loops. Geol. Soc. Am. Bull. 85, 581–586.
Bridge, J.S., Alexander, J., Collier, R.E.L., Gawthorpe, R.L., Jarvis, J., 1995. Ground-penetrating radar and coring used to study the large-scale structure of point-bar deposits in three dimensions. Sedimentology 42, 839–852.
Bridges, P.H., Leeder, M.R., 1976. Sedimentary model for intertidal mudflat channels, with examples from the Solway Firth, Scotland. Sedimentology 23, 533–552. https://doi.org/10.1111/j.1365-3091.1976.tb00066.x
Brivio, L., Ghinassi, M., D'Alpaos, A., Finotello, A., Fontana, A., Roner, M., Howes,

N., 2016. Aggradation and lateral migration shaping geometry of a tidal point bar: An example from salt marshes of the Northern Venice Lagoon (Italy). Sediment. Geol. 343, 141–155. https://doi.org/10.1016/j.sedgeo.2016.08.005

Candel, J.H.J., Makaske, B., Storms, J.E.A., Wallinga, J., 2017. Oblique aggradation: A novel explanation for sinuosity of low-energy streams in peat-filled valley systems. Earth Surf. Process. Landforms 42, 2679–2696. https://doi.org/10.1002/esp.4100

Carniello, L., D'Alpaos, A., Defina, A., 2011. Modeling wind waves and tidal flows in shallow micro-tidal basins. Estuar. Coast. Shelf Sci. 92, 263–276. https://doi.org/10.1016/j.ecss.2011.01.001

Carniello, L., D'Alpaos, A., Botter, G., Rinaldo, A., 2016. Statistical characterization of spatiotemporal sediment dynamics in the Venice lagoon. J. Geophys. Res. Earth Surf. 121, 1049–1064. https://doi.org/10.1002/2015JF003793.Received

Carniello, L., Defina, A., D'Alpaos, L., 2009. Morphological evolution of the Venice lagoon: Evidence from the past and trend for the future. J. Geophys. Res. Earth Surf. 114, 1–10. https://doi.org/10.1029/2008JF001157

Choi, K., Jo, J., 2015. Morphodynamics and stratigraphic architecture of compound dunes on the open-coast macrotidal flat in the northern Gyeonggi Bay, west coast of Korea. Mar. Geol. 366, 34–48. https://doi.org/10.1016/j.margeo.2015.05.002

Colombera, L., Mountney, N.P., Russell, C.E., Shiers, M.N., McCaffrey, W.D., 2017. Geometry and compartmentalization of fluvial meander-belt reservoirs at the bar-form scale: Quantitative insight from outcrop, modern and subsurface analogues. Mar. Pet. Geol. 82, 35–55. https://doi.org/10.1016/j.marpetgeo.2017.01.024

Crosato, A., 2009. Physical explanations of variations in river meander migration rates from model comparison. Earth Surf. Process. Landforms 34, 2078–2086. https://doi.org/10.1002/esp.1898

D'Alpaos, A., Carniello, L., Rinaldo, A., 2013. Statistical mechanics of wind wave-induced erosion in shallow tidal basins: Inferences from the Venice Lagoon. Geophys. Res. Lett. 40, 3402–3407. https://doi.org/10.1002/grl.50666

D'Alpaos, A., Ghinassi, M., Finotello, A., Brivio, L., Bellucci, L.G., Marani, M., 2017. Tidal meander migration and dynamics: A case study from the Venice Lagoon. Mar. Pet. Geol. 87, 80–90. https://doi.org/10.1016/j.marpetgeo.2017.04.012

D'Alpaos, A., Lanzoni, S., Marani, M., Fagherazzi, S., Rinaldo, A., 2005. Tidal network ontogeny: Channel initiation and early development. J. Geophys. Res. Earth Surf. 110, 1–14. https://doi.org/10.1029/2004JF000182

D'Alpaos, A., Lanzoni, S., Marani, M., Rinaldo, A., 2010. On the tidal prism-channel area relations. J. Geophys. Res. Earth Surf. 115, 1–13. https://doi.org/10.1029/2008JF001243

D'Alpaos, A., Lanzoni, S., Marani, M., Rinaldo, A., 2007. Landscape evolution in tidal embayments: Modeling the interplay of erosion, sedimentation, and vegetation dynamics. J. Geophys. Res. Earth Surf. 112, 1–17. https://doi.org/10.1029/2006JF000537

D'Alpaos, L., 2010. Fatti e misfatti di idraulica lagunare. La laguna di Venezia dalla diversione dei fiumi alle nuove opere alle bocche di porto, Venezia: Istituto Veneto di Scienze, Lettere ed Arti.

Dalrymple, R.W., Makino, Y., Zaitlin, B.., 1991. Temporal and spatial patterns of rhythmite deposition on mud flats in the macrotidal Cobequid Bay-Salmon River estuary. Bay of Fundy, Canada. Clastic Tidal Sedimentol. 16, 137–160.

Day, J.W., Rismondo, A., Scarton, F., Are, D., Cecconi, G., 1998. Relative sea level rise and Venice lagoon wetlands. J. Coast. Conserv. 4, 27–34.

De Mowbray, T., 1983. The genesis of lateral accretion deposits in recent intertidal mudflat channels, Solway Firth, Scotland. Sedimentology 30, 425–435. https://doi.org/10.1111/j.1365-3091.1983.tb00681.x

Dietrich, W.E., Smith, J.D., 1984. Processes controlling the equilibrium bed morphology in river meanders, in: River Meandering: Proceedings of the Conference Rivers '83. pp. 759–769.

Dietrich, W.E., Smith, J.D., Dunne, T., 1979. Flow and Sediment Transport in a Sand Bedded Meander. J. Geol. 87, 305–315. https://doi.org/10.1086/628419

Donnici, S., Madricardo, F., Serandrei-Barbero, R., 2017. Sedimentation rate and lateral migration of tidal channels in the Lagoon of Venice (Northern Italy). Estuar. Coast. Shelf Sci. 198, 354–366. https://doi.org/10.1016/j.ecss.2017.02.016

Durkin, P.R., Hubbard, S.M., Boyd, R.L., Leckie, D.A., 2015. Stratigraphic Expression of Intra-Point-Bar Erosion and Rotation. J. Sediment. Res. 85, 1238–1257. https://doi.org/10.2110/jsr.2015.78

Elliott, R.E., 1985. Quantification of peat to coal compaction stages, based especially on phenomena in the East Pennine Coalfield, England. Proc. Yorksh. Geol. Soc. 45, 163–172.

Fagherazzi, S., Gabet, E.J., Furbish, D.J., 2004. The effect of bidirectional flow on tidal channel planforms. Earth Surf. Process. Landforms 29, 295–309. https://doi.org/10.1002/esp.1016

Finotello, A., Lanzoni, S., Ghinassi, M., Marani, M., Rinaldo, A., D'Alpaos, A., 2018. Field migration rates of tidal meanders recapitulate fluvial morphodynamics.

Proc. Natl. Acad. Sci. 115, 1463–1468. https://doi.org/10.1073/pnas.1711330115

Fisk, H.N., 1944. Geological Investigation of the Alluvial Valley of the Lower Mississippi River. US Army Corps Eng. Mississippi River Comm. 1–78.

Fontana, A., Mozzi, P., Marchetti, M., 2014. Alluvial fans and megafans along the southern side of the Alps. Sediment. Geol. 301, 150–171. https://doi.org/10.1016/j.sedgeo.2013.09.003

Frothingham, K.M., Rhoads, B.L., 2003. Three-dimensional flow structure and channel change in an asymmetrical compound meander loop, Embarras River, Illinois. Earth Surf. Process. Landforms 28, 625–644. https://doi.org/10.1002/esp.471

Fruergaard, M., Andersen, T.J., Nielsen, L.H., Madsen, A.T., Johannessen, P.N., Murray, A.S., Kirkegaard, L., Pejrup, M., 2011. Punctuated sediment record resulting from channel migration in a shallow sand-dominated micro-tidal lagoon, Northern Wadden Sea, Denmark. Mar. Geol. 280, 91–104. https://doi.org/10.1016/j.margeo.2010.12.003

Gabet, E.J., 1998. Lateral Migratiion and Bank Erosion in a Saltmarsh Tidal Channel in San Francisco Bay, California. Estuaries 21, 745–753. https://doi.org/10.2307/1353278

Garofalo, D., 1980. The Influence of Wetland Vegetation on Tidal Stream Channel Migration and Morphology. Estuaries 3, 258–270. https://doi.org/10.2307/1352081

Gatto, P., Carbognin, L., 1981. The lagoon of Venice: Natural environmental trend and man-induced modification. Hydrol. Sci. Bull. 26, 379–391. https://doi.org/10.1080/02626668109490902

Ghinassi, M., Brivio, L., D'Alpaos, A., Finotello, A., Carniello, L., Marani, M., Cantelli, A., 2018a. Morphodynamic evolution and sedimentology of a microtidal meander bend of the Venice Lagoon (Italy). Mar. Pet. Geol. 96, 391–404. https://doi.org/10.1016/j.marpetgeo.2018.06.011

Ghinassi, M., Ielpi, A., Aldinucci, M., Fustic, M., 2016. Downstream-migrating fluvial point bars in the rock record. Sediment. Geol. 334, 66–96. https://doi.org/10.1016/j.sedgeo.2016.01.005

Ghinassi, M., Moody, J.A., Martin, D., 2018b. Influence of extreme and annual floods on point-bar sedimentation: Inferences from Powder River , Montana , USA. Geol. Soceity Am. Bull. 1–13. https://doi.org/10.1130/B31990.1/4292202/b31990.pdf

Ghinassi, M., Nemec, W., Aldinucci, M., Nehyba, S., Ozaksoy, V., Fidolini, F., 2014. Plan-form evolution of ancient meandering rivers reconstructed from longitudinal outcrop sections. Sedimentology 61, 952–977. https://doi.org/10.1111/sed.12081

Gobo, K., Ghinassi, M., Nemec, W., 2015. Gilbert-type deltas recording short-term base-level changes: Delta-brink morphodynamics and related foreset facies. Sedimentology 62, 1923–1949. https://doi.org/10.1111/sed.12212

Green, M.O., Coco, G., 2007. Sediment transport on an estuarine intertidal flat: Measurements and conceptual model of waves, rainfall and exchanges with a tidal creek. Estuar. Coast. Shelf Sci. 72, 553–569. https://doi.org/10.1016/j.ecss.2006.11.006

Helland-Hansen, W., Hampson, G.J., 2009. Trajectory analysis: Concepts and applications. Basin Res. 21, 454–483. https://doi.org/10.1111/j.1365-2117.2009.00425.x

Henriksen, S., Hampson, G.J., Helland-Hansen, W., Johannessen, E.P., Steel, R.J., 2009. Shelf edge and shoreline trajectories, a dynamic approach to stratigraphic analysis. Basin Res. 21, 445–453. https://doi.org/10.1111/j.1365-2117.2009.00432.x

Henriksen, S., Helland-hansen, W., Bullimore, S., 2011. Relationships between shelf-edge trajectories and sediment dispersal along depositional dip and strike: a different approach to sequence stratigraphy. Basin Res. 23, 3–21. https://doi.org/10.1111/j.1365-2117.2010.00463.x

Hooke, J.M., 1984. Changes in river meanders: a review of techniques and results of analyses. Prog. Phys. Geogr. Earth Environ. 8, 473–508. https://doi.org/10.1177/030913338400800401

Hooke, R.L.B., 1975. Distribution of sediment transport and shear stress in a meander bend. J. Geol. 83, 543–565.

Hudson, P.F., Kesel, R.H., 2000. Channel migration and meander-bend curvature in the lower Mississippi River prior to major human modification. Geology 28, 531–534. https://doi.org/10.1130/0091-7613(2000)28<531:CMAMCI>2.0.CO;2

Hughes, Z.J., 2012. Tidal Channels on Tidal Flats and Marshes, in: Davis, R.A., Dalrymple, R.W. (Eds.), Principles of Tidal Sedimentology. pp. 269–300. https://doi.org/10.1007/978-94-007-0123-6

Ielpi, A., Ghinassi, M., 2014. Planform architecture, stratigraphic signature and morphodynamics of an exhumed Jurassic meander plain (Scalby Formation, Yorkshire, UK). Sedimentology 61, 1923–1960. https://doi.org/10.1111/sed.12122

Ielpi, A., Gibling, M.R., Bashforth, A.R., Dennar, C.I., 2015. Impact of Vegetation On Early Pennsylvanian Fluvial Channels: Insight From the Joggins Formation of

Atlantic Canada. J. Sediment. Res. 85, 999–1018. https://doi.org/10.2110/jsr.2015.50

Jackson, R.G.I., 1976. Depositional model of point bars in the Lower Wabash River. J. Sediment. Petrol. 46, 579–594.

Kent, D. V., Rio, D., Massari, F., Kukla, G., Lanci, L., 2002. Emergence of Venice during the Pleistocene. Quat. Sci. Rev. 21, 1719–1727. https://doi.org/10.1016/S0277-3791(01)00153-6

Lagasse, P.F., Zevenbergen, L.W., Spitz, W.J., Thorne, C.R., 2004. Methodology for Predicting Channel Migration. NCHRP Proj. No. 24-16 . Ayres Assoc. Inc. - Fort Collins, Color. https://doi.org/10.17226/23352

Lanzoni, S., Seminara, G., 2002. Long-term evolution and morphodynamic equilibrium of tidal channels. J. Geophys. Res. Ocean. 107, 3001. https://doi.org/10.1029/2000JC000468

Larue, D.K., Martinez, P.A., 1989. Use of bed-form climb models to analyze geometry and preservation potential of clastic facs and erosional surfaces. Am. Assoc. Pet. Geol. Bull. 73, 40–53.

Long, A.J., Waller, M.P., Stupples, P., 2006. Driving mechanisms of coastal change: Peat compaction and the destruction of late Holocene coastal wetlands. Mar. Geol. 225, 63–84. https://doi.org/10.1016/j.margeo.2005.09.004

Makaske, B., 2001. Anastomosing rivers: A review of their classification, origin and sedimentary products. Earth Sci. Rev. 53, 149–196. https://doi.org/10.1016/S0012-8252(00)00038-6

Marani, M., D’Alpaos, A., Lanzoni, S., Carniello, L., Rinaldo, A., 2007. Biologically-controlled multiple equilibria of tidal landforms and the fate of the Venice lagoon. Geophys. Res. Lett. 34, 1–5. https://doi.org/10.1029/2007GL030178

Marani, M., Lanzoni, S., Zandolin, D., Seminara, G., Rinaldo, A., 2002. Tidal meanders. Water Resour. Res. 38, 7-1-7–14. https://doi.org/10.1029/2001WR000404

Massari, F., Grandesso, P., Stefani, C., Jobstraibizer, P.G., 2009. A small polyhistory foreland basin evolving in a context of oblique convergence: the Venetian basin (Chattian to Recent, Southern Alps, Italy), in: Allen, P.A., Homewood, P. (Eds.), Foreland Basins. pp. 141–168. https://doi.org/10.1002/9781444303810

Massari, F., Rio, D., Serandrei Barbero, R., Asioli, A., Capraro, L., Fornaciari, E., Vergerio, P.P., 2004. The environment of Venice area in the past two million years. Palaeogeogr. Palaeoclimatol. Palaeoecol. 202, 273–308. https://doi.org/10.1016/S0031-0182(03)00640-0

McClennen, C.E., Housley, R.A., 2006. Late-Holocene Channel Meander Migration and Mudflat Accumulation Rates, Lagoon of Venice, Italy. J. Coast. Res. 22, 930–945. https://doi.org/10.2112/03-0113.1

McGowen, J.H., Garner, L.E., 1970. Physiographic Features and Stratification Types of Coarse-Grained Pointbars: Modern and Ancient Examples. Sedimentology 14, 77–111. https://doi.org/10.1111/j.1365-3091.1970.tb00184.x

Miall, A.D., 1985. Architectural-element analysis: A new method of facies analysis applied to fluvial deposits. Earth-Science Rev. 22, 261–308. https://doi.org/10.1016/0012-8252(85)90001-7

Moody, J.A., Meade, R.H., 2014. Ontogeny of point bars on a river in a cold semi-arid climate. Bull. Geol. Soc. Am. 126, 1301–1316. https://doi.org/10.1130/B30992.1

Morris, J.T., Sundareshwar, P. V, Nietch, C.T., Kjerfve, B., Cahoon, D.R., 2002. Responses of Coastal Wetlands To Rising Sea Level. Ecology 83, 2869–2877.

Mudd, S.M., D'Alpaos, A., Morris, J.T., 2010. How does vegetation affect sedimentation on tidal marshes? Investigating particle capture and hydrodynamic controls on biologically mediated sedimentation. J. Geophys. Res. Earth Surf. 115, 1–14. https://doi.org/10.1029/2009JF001566

Nanson, G.C., Croke, J.C., 1992. A genetic classification of floodplains. Geomorphology 4, 459–486.

Nanson, G.C., Hickin, E.J., 1986. A statistical analysis of bank erosion and channel migration in western Canada. Geol. Soc. Am. Bull. 97, 497–504. https://doi.org/10.1130/0016-7606(1986)97<497:ASAOBE>2.0.CO;2

Pranter, M.J., Ellison, A.I., Cole, R.D., Patterson, P.E., 2007. Analysis and modeling of intermediate-scale reservoir heterogeneity based on a fluvial point-bar outcrop analog, Williams Fork Formation, Piceance Basin, Colorado. Am. Assoc. Pet. Geol. Bull. 91, 1025–1051. https://doi.org/10.1306/02010706102

Puigdefabregas, C., 1973. Miocene point bar deposits in the Ebro Basin, Northern Spain. Sedimentology 20, 133–144.

Puigdefabregas, C., Van Vliet, A., 1977. Meandering stream deposits from the Tertiary of the Southern Pyrenees. Fluv. Sedimentol. Mem. 5 5, 469–485.

Rajchl, M., Uličný, D., 2005. Depositional record of an avulsive fluvial system controlled by peat compaction (Neogene, Most Basin, Czech Republic). Sedimentology 52, 601–625. https://doi.org/10.1111/j.1365-3091.2005.00691.x

Rieu, R., van Heteren, S., Van der Spek, A.J.F., De Boer, P.L., 2005. Development and preservation of a Mid-Holocene tidal-channel network offshore the Western Netherlands. J. Sediment. Res. 75, 409–419. https://doi.org/10.21110/jsr.2005.032

Roner, M., D'Alpaos, A., Ghinassi, M., Marani, M., Silvestri, S., Franceschinis, E., Realdon, N., 2016. Spatial variation of salt-marsh organic and inorganic deposition and organic carbon accumulation: Inferences from the Venice lagoon, Italy. Adv. Water Resour. 93, 276–287. https://doi.org/10.1016/j.advwatres.2015.11.011

Roner, M., Ghinassi, M., Fedi, M., Liccioli, L., Bellucci, L.G., Brivio, L., D'Alpaos, A., 2017. Latest Holocene depositional history of the southern Venice Lagoon, Italy. The Holocene 27, 1731–1744. https://doi.org/10.1177/0959683617708450

Silvestri, S., Defina, A., Marani, M., 2005. Tidal regime, salinity and salt marsh plant zonation. Estuar. Coast. Shelf Sci. 62, 119–130. https://doi.org/10.1016/j.ecss.2004.08.010

Smith, D.G., 1987. Meandering river point bar lithofacies models: modern and ancient examples compared, in: Ethridge, F.G., Flores, R.M., Harvey, M.D. (Eds.), Recent Developments in Fluvial Sedimentology: Contributions from the Third International Fluvial Sedimentology Conference. SEPM Society for Sedimentary Geology, pp. 83–91.

Smith, D.G., Hubbard, S.M., Leckie, D.A., Fustic, M., 2009. Counter point bar deposits: Lithofacies and reservoir significance in the meandering modern peace river and ancient McMurray formation, Alberta, Canada. Sedimentology 56, 1655–1669. https://doi.org/10.1111/j.1365-3091.2009.01050.x

Stefanon, L., Carniello, L., D'Alpaos, A., Rinaldo, A., 2012. Signatures of sea level changes on tidal geomorphology: Experiments on network incision and retreat. Geophys. Res. Lett. 39, 1–6. https://doi.org/10.1029/2012GL051953

Terwindt, J.H.J., 1988. Palaeotidal reconstructions of inshore tidal depositional environments, in: De Boer, P.L., van Gelder, A., Nio, S.-D. (Eds.), Tide-Influenced Sedimentary Environments. pp. 233–263.

Toonen, W.H.J., Kleinhans, M.G., Cohen, K.M., 2012. Sedimentary architecture of abandoned channel fills. Earth Surf. Process. Landforms 37, 459–472. https://doi.org/10.1002/esp.3189

Törnqvist, T.E., Wallace, D.J., Storms, J.E.A., Wallinga, J., Van Dam, R.L., Blaauw, M., Derksen, M.S., Klerks, C.J.W., Meijneken, C., Snijders, E.M.A., 2008. Mississippi Delta subsidence primarily caused by compaction of Holocene strata. Nat. Geosci. 1, 173–176. https://doi.org/10.1038/ngeo129

Tosi, L., Rizzetto, F., Bonardi, M., Donnici, S., Serandrei-Barbero, R., Toffoletto, F., 2007. Note Illustrative della Carta Geologica d'Italia alla scala 1:50.000. foglio 148-149, Chioggia-Malamocco.

van Asselen, S., 2011. The contribution of peat compaction to total basin subsidence: Implications for the provision of accommodation space in organic-rich deltas. Basin Res. 23, 239–255. https://doi.org/10.1111/j.1365-2117.2010.00482.x

van Asselen, S., Stouthamer, E., Smith, N.D., 2010. Factors Controlling Peat Compaction in Alluvial Floodplains: A Case Study in the Cold-Temperate Cumberland Marshes, Canada. J. Sediment. Res. 80, 155–166. https://doi.org/10.2110/jsr.2010.015

van de Lageweg, W.I., Schuurman, F., Cohen, K.M., van Dijk, W.M., Shimizu, Y., Kleinhans, M.G., 2016. Preservation of meandering river channels in uniformly aggrading channel belts. Sedimentology 63, 586–608. https://doi.org/10.1111/sed.12229

Willis, B.J., Tang, H., 2010. Three-Dimensional Connectivity of Point-Bar Deposits. J. Sediment. Res. 80, 440–454. https://doi.org/10.2110/jsr.2010.046

Zecchin, M., Baradello, L., Brancolini, G., Donda, F., Rizzetto, F., Tosi, L., 2008.

Sequence stratigraphy based on high-resolution seismic profiles in the late Pleistocene and Holocene deposits of the Venice area. Mar. Geol. 253, 185–198. https://doi.org/10.1016/j.margeo.2008.05.010

Zecchin, M., Brancolini, G., Tosi, L., Rizzetto, F., Caffau, M., Baradello, L., 2009. Anatomy of the Holocene succession of the southern Venice lagoon revealed by very high-resolution seismic data. Cont. Shelf Res. 29, 1343–1359. https://doi.org/10.1016/j.csr.2009.03.006

Zecchin, M., Tosi, L., Caffau, M., Baradello, L., Donnici, S., 2014. Sequence stratigraphic significance of tidal channel systems in a shallow lagoon (Venice, Italy). The Holocene 24, 646–658. https://doi.org/10.1177/0959683614526903